# Multilayer Nonlinear Processing for Information Privacy in Sensor Networks

Xin He, Meng Sun, *Student Member, IEEE*, Wee Peng Tay, *Senior Member, IEEE*, and Yi Gong, *Senior Member, IEEE*



***Abstract*—A sensor network wishes to transmit information to a fusion center to allow it to detect a public hypothesis, but at the same time prevent it from inferring a private hypothesis. We propose a multilayer nonlinear processing procedure at each sensor to distort the sensor's data before it is sent to the fusion center. In our proposed framework, sensors are grouped into clusters, and each sensor first applies a nonlinear fusion function on the information it receives from sensors in the same cluster and in a previous layer. A linear weighting matrix is then used to distort the information it sends to sensors in the next layer. We adopt a nonparametric approach and develop a modified mirror descent algorithm to optimize the weighting matrices so as to ensure that the regularized empirical risk of detecting the private hypothesis is above a given privacy threshold, while minimizing the regularized empirical risk of detecting the public hypothesis. Experiments on empirical datasets demonstrate that our approach is able to achieve a good trade-off between the error rates of the public and private hypothesis.**

***Index Terms*—Internet of Things, information privacy, nonparametric detection, sensor networks.**

## I. Introduction

With the popularity of Internet of Things (IoT) devices like on-body sensors, smart home appliances, and smart phones [1]–[4], massive amounts of data about users' habits, routines and preferences are being collected by service providers. Sensors make observations, and sends their data to a fusion center [5]–[8] to allow service providers to perform inferences that can potentially improve the quality of life. However, the same data can also be exploited to learn users' private behaviors, habits, lifestyle choices, or health conditions. An example of a sensor network is illustrated in Fig. 1. The sensor network can be an on-body sensor network, where the distributed sensors include inertial measurement units (IMU), electrocardiography (ECG), skin conductivity (SC) sensors and respiration sensors, sending data to a fitness monitoring service provider or fusion center. The IMU records motion acceleration information, which can be used for activity classification. The ECG signal and the data from the SC and respiration sensors can be used for stress level detection. The sensor data may be used to monitor the stress level and exercising habits of the user.

This research is supported in part by the Singapore Ministry of Education Academic Research Fund Tier 2 grant MOE2014-T2-1-028, and in part by Natural Science Foundation of Guangdong Province under Grant No. 2015A030313844.

Xin He and Yi Gong are with the Department of Electrical and Electronic Engineering, Southern University of Science and Technology, Shenzhen, China. Email: hx66hx@gmail.com, gongy@sustc.edu.cn. Meng Sun and Wee Peng Tay are with the Department of Electrical and Electronic Engineering, Nanyang Technological University, Singapore. Email: MSUN002@e.ntu.edu.sg, wptay@ntu.edu.sg.

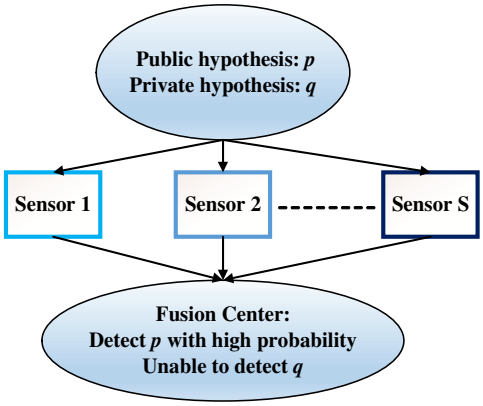


Fig. 1. Information privacy in sensor networks.

These constitute the public hypothesis or inference the service provider is authorized to perform. However, the same data may also be used to discover some latent health issues of the user, which constitute the private information. Since both public and private information are embedded in the observed data, distorting the observed data before sending to the fusion center is crucial in protecting users' privacy. Our goal is to distort the data in such a way that the fusion center can still infer the public information, while making it difficult for the fusion center to infer the private information.

As the number of IoT devices is increasing, ensuring users' privacy has gained traction in both the IoT industry and research community. For instance, Apple Inc. has recently announced that it will incorporate differential privacy mechanisms into its data collection process [9]. However, most privacy preserving mechanisms like those based on differential privacy, encryption or perturbation [10]–[12], [12]–[19] proposed in the literature concerns data privacy, i.e., the prevention of any statistical algorithms operating on the data from inferring much about each individual datum. For example, the paper [20] proposes a convolution deep learning approach to locate and blur the sensitive objects in an image. This approach assumes the private or sensitive objects are separable from the rest of the image. However, both public and private information are often embedded in the same datum in many situations. For example, information about both the emotions and medical condition of a person are embedded in the same ECG signal. Furthermore, by blurring the sensitive object in an image indicates that such an object is present, and may result in some privacy leakage.

We call the prevention of statistical inference *information privacy*. A technical definition for information privacy was first proposed by [21]. A minimax formulation was proposed by [22], [23] to design privacy mappings or filters that are robust to inference attacks. However, [22], [23] do not address the information privacy metric of [21]. A nonparametric approach in which data is first sanitized by mapping to a subspace was proposed by [24], [25]. However, this approach is impractical in a decentralized sensor network since the sanitization can only be done by a trusted data curator who first aggregates data from all sensors. Furthermore, no theoretical guarantees for the level of information privacy achievable are available. Practical nonparametric approaches to achieve information privacy in the sense of [21] for decentralized sensor networks were developed in [26], [27]. In [26], a nonlinear probabilistic mapping is used to distort each sensor's local observations before being sent to the fusion center. This mapping is designed to prevent the fusion center from inferring about a private hypothesis, while still allowing it to detect a public hypothesis. However, finding the optimal mappings becomes computationally complex when the range of the mapping is large. In [27], a low complexity linear precoder at each sensor is used instead. By tuning the linear precoder, the fusion center is again prevented from inferring a private hypothesis. However, in some cases, the error detection rate of the public hypothesis may deteriorate significantly.

In this paper, we propose a multilayer sensor network architecture to achieve a better trade-off between information privacy and inference of the public hypothesis. Our inspiration comes from neural networks, a multilayer nonlinear structure that has been validated in various applications to be a flexible representation system for feature extraction and learning [28], [29]. Our experiments suggest that using a multilayer nonlinear structure in a sensor network has the potential to balance the distortion in information related to the private hypothesis and the representation of the public hypothesis. In particular, information from one layer of sensors is first linearly weighted with a weighting matrix before sending to all sensors in the next layer. Each sensor in the next layer then uses a nonlinear function to fuse the information it has received, before repeating the procedure. The nonlinear fusion function is fixed, but the weighting matrices are optimized so that detecting the private hypothesis at the final fusion center is difficult, while keeping the accuracy of detecting the public hypothesis reasonable. Our optimization framework can be shown to achieve information privacy with high probability. However, our optimization formulation is a non-convex program. We therefore propose a modified mirror descent method to solve it. We verify the performance of our proposed approach on three real datasets, which reveal the impact of various factors like the privacy threshold, the choice of the nonlinear distortion function, and the number of layers, on the trade-off between the detection rate of the public hypothesis and that of the private hypothesis.

A preliminary version of this paper appears in [30]. Our previous work utilizes the traditional empirical risk minimization approach commonly used in the machine learning literature [31], [32]. However, in this paper, we adopt an empirical normalized risk metric, which can be shown to achieve information privacy with high probability. Furthermore, we have generalized our optimization framework and provided a modified mirror descent method to implement it.

The rest of this paper is organized as follows. In Section II, we first present our system model and assumptions. We then present our proposed multilayer nonlinear processing framework. In Section III, we present an algorithm to design the multilayer weighting matrices. Simulation results are presented in Section IV, and Section V concludes the paper.

*Notations.* We use boldface letters to represent vectors and matrices. The $i$-th component of a vector $\boldsymbol{\alpha}$ is denoted as $\boldsymbol{\alpha}(i)$. The superscript $^T$ denotes matrix transpose, and $\mathbb{R}$ is the set of real numbers. We use $\|\mathbf{G}\|_F$ to denote the Frobenius norm of $\mathbf{G}$. The operator $\mathrm{vec}(\cdot)$ is the vectorization operation, while $\mathrm{Diag}\,(\mathbf{y})$ denotes a diagonal matrix with the vector $\mathbf{y}$ on its diagonal. We use $\circ$ to denote Kronecker product. The symbol $\mathbf{1}_{\{A\}}$ is the indicator function with value 1 iff the clause $A$ is true. Throughout this paper, we assume all random variables have either probability density or mass functions, and are defined on a common underlying probability space with probability measure $\mathbb{P}$. We use $\mathsf{p}_X$ to denote the probability density or mass function of the random variable $X$, and $\mathsf{p}_{X|Y}$ to denote the conditional probability density or mass function of $X$ given $Y$.

## II. System Model

In this section, we present our system model and assumptions. We propose a multilayer nonlinear processing architecture, and present the concept of information privacy. We then formulate an optimization problem for our multilayer architecture with an empirical normalized risk privacy constraint, which allows us to achieve information privacy with high probability.

### A. Multilayer Architecture

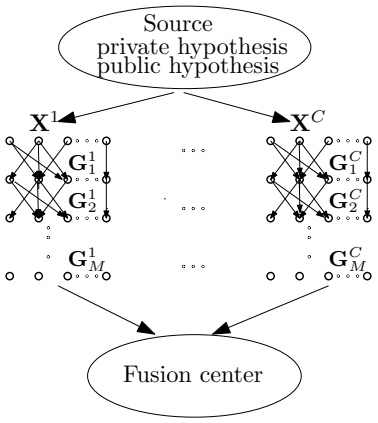


Fig. 2. **Distributed multilayer nonlinear process.**

Let $p$ and $q$ be two binary hypotheses, each taking value in $\{-1, 1\}$. The hypothesis $p$ is the public binary hypothesis that a sensor network wants the fusion center to detect, while $q$ is a private binary hypothesis whose true state the sensor

network wishes to protect from the fusion center. To avoid trivial scenarios, we assume that $\min\{\mathsf{p}_q(1), \mathsf{p}_q(-1)\} > 0$.

Consider the multilayer sensor network shown in Fig. 2. Sensors are clustered into $C$ clusters. For each cluster $c \in \{1, \ldots, C\}$, suppose there are $n_c$ sensors each observing a row vector of length $k$. Let $\mathbf{X}^c \in \mathbb{R}^{n_c \times k}$ be the collection of all sensor observations in the first layer of cluster $c$, which is distributed according to an unknown distribution depending on a pair of hypotheses $(p, q)$. Each sensor in the first layer applies a linear transformation on its local observation before sending that to sensors in the second layer. Let $\mathbf{G}_1^c \in \mathbb{R}^{d \times n_c}$ be the (aggregated) weighting matrix or linear precoder used by the sensors in the first layer so that each sensor in the second layer receives $\mathbf{G}_1^c \mathbf{X}^c$. Each sensor in the second layer then applies a nonlinear fusion function $h : \mathbb{R}^{d \times k} \to \mathbb{R}^{d \times k}$ to $\mathbf{G}_1^c \mathbf{X}^c$. We assume that $h(\cdot)$ operates element-wise on each element of its input argument. Each sensor then weighs the output of $h(\cdot)$ with $\mathbf{G}_2^c \in \mathbb{R}^{d \times d}$ before sending $\mathbf{G}_2^c h(\mathbf{G}_1^c \mathbf{X}^c)$ to sensors in the third layer. This process is repeated until the fusion center receives

$$\mathbf{Z}^c(\mathbf{G}^c, \mathbf{X}^c) = \mathrm{vec}(\mathbf{G}_M^c h(\mathbf{G}_{M-1}^c h(\cdots h(\mathbf{G}_1^c \mathbf{X}^c)))), \quad (1)$$

where $M$ is the number of layers in the network, and $\mathbf{G}^c = \{\mathbf{G}_m^c\}_{m=1}^M$. Let $\mathbf{X} = \{\mathbf{X}^c : c = 1, \ldots, C\}$. The fusion center makes its inferences based on the received information

$$\mathbf{Z}(\mathbf{X}) = [\mathbf{Z}^1(\mathbf{G}^1, \mathbf{X}^1); \ldots; \mathbf{Z}^C(\mathbf{G}^C, \mathbf{X}^C)], \quad (2)$$

which is called the *sanitized* information. The nonlinear function $h(\cdot)$ is fixed, but our goal is to choose $\mathbf{G}^c$, $c = 1, \ldots, C$, to make it difficult for the fusion center to detect the private hypothesis $q$, while still having a reasonable accuracy in detecting $p$. We assume that $h(\cdot)$ and $\mathbf{G}^c$, $c = 1, \ldots, C$, are chosen such that the following assumption holds.

**Assumption 1.** *The received sanitized information at the fusion center $\mathbf{Z}(\mathbf{X}) \in \mathbb{U} \subset \mathbb{R}^{dkC}$, where $\mathbb{U}$ is a compact set.*

The above assumption can be satisfied by normalizing the data input $\mathbf{X}^c$ and imposing appropriate restrictions on each $\mathbf{G}^c$ (cf. Section III).

In many applications, we do not know the underlying distributions relating the sensor observations and the hypotheses. Instead, we are given a training set $(\mathbf{X}_i, p_i, q_i)_{i=1}^N$, where each $(\mathbf{X}_i, p_i, q_i)$ is an independent and identically distributed (i.i.d.) realization of $(\mathbf{X}, p, q)$.[1] Let $\mathbf{Z}_i = \mathbf{Z}(\mathbf{X}_i)$. We assume that the fusion center has access to the training samples $(\mathbf{Z}_i, p_i, q_i)_{i=1}^N$, and trains a Tikhonov regularized empirical risk function [31] as a classifier for $p$, subject to an empirical risk privacy constraint for $q$, which we describe in Section II-B below.

In practice, it may not be practical to have multiple layers of physical sensors as shown in Fig. 2. However, our proposed architecture is general enough to encompass different physical interpretations, including architectures in which part of the layers shown in Fig. 2 are "virtualized". For example, each layer in a cluster can be physically implemented within a single sensor, so that a cluster consists of a tandem of several nodes (see Fig. 3). In this scenario, each node in the first layer corresponds to an observation time instance of the first sensor in the cluster, and the observations form a time series for the first sensor. In another example, a cluster may correspond physically to a single sensor (see Fig. 4), so that the multilayer nonlinear processing architecture is implemented as internal on-board processing within the sensor. Note that since we adopt a machine learning approach, we have not assumed any independence structure between sensor observations in our framework, and we allow sensor observations to be correlated.

[1]Throughout this paper, we use superscript to refer to a sensor or cluster index, and the subscript index $i$ to refer to the $i$-th training data sample.

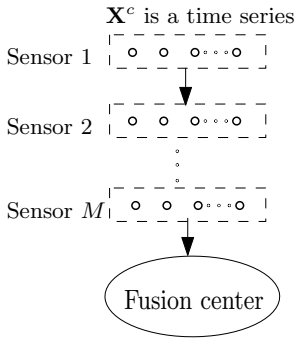


Fig. 3. Each layer in cluster $c$ corresponds to a single sensor.

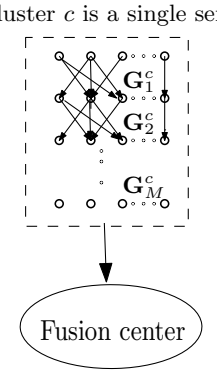


Fig. 4. Cluster $c$ corresponds to a single sensor, with the multilayer processing architecture implemented within the sensor.

### B. Information Privacy

Consider the Markov chain $q \to \mathbf{X} \to \mathbf{Z}(\mathbf{X})$, where $\mathbf{Z}(\mathbf{X})$ is the information received by the fusion center. In order to prevent the fusion center inferring about $q$ from $\mathbf{Z}(\mathbf{X})$, we aim to design the mapping $\mathbf{Z}(\cdot)$ such that the posterior distribution of $q$ given $\mathbf{Z}(\mathbf{X})$ does not differ significantly from the prior distribution of $q$. We adopt the following information privacy definition.

**Definition 1** ($(\epsilon, \delta)$-information privacy)**.** *For $\epsilon > 0$ and $\delta \in [0, 1]$, we say that $q$ given $\mathbf{Z}$ or its conditional probability mass function $\mathsf{p}_{q|\mathbf{Z}}$ has $(\epsilon, \delta)$-information privacy if*

$$\mathbb{P}\left(e^{-\epsilon} \leq \frac{\mathsf{p}_{q|\mathbf{Z}}(q \mid \mathbf{Z})}{\mathsf{p}_q(q)} \leq e^{\epsilon}\right) \geq 1 - \delta.$$

In the case where $\delta = 0$, the above definition is equivalent to the notion of $\epsilon$-information privacy proposed by [21]. Since we do not know the underlying joint distribution governing the sensor observations and hypotheses *a priori*, and instead depend on a training sample set to determine the mapping $\mathbf{Z}(\cdot)$, we cannot hope to achieve information privacy with $\delta = 0$. Therefore, in the following, our goal is to develop a privacy metric that allows us to achieve $(\epsilon, \delta)$-information privacy for any $\epsilon > 0$ and $\delta \in (0, 1)$, if the number of training samples is sufficiently large. Following [33], [34], let $\phi$ be a convex loss function, $\mathcal{H}$ be a reproducing kernel Hilbert space (RKHS) with kernel $\kappa(\cdot, \cdot)$, kernel inner product $\langle \cdot, \cdot \rangle$, and associated norm $\|\cdot\|$. We restrict the rule used by the fusion center to infer $p$ and $q$ based on $\mathbf{Z}$ to be of the form $\langle w, \Phi(\mathbf{Z}) \rangle$, where $\Phi(\mathbf{Z}) = \kappa(\cdot, \mathbf{Z})$ is the feature map of $\mathcal{H}$. We seek to minimize the empirical $\phi$-risk of deciding $p$ while preserving information privacy. Let $\mathbf{G} = \{\mathbf{G}^c\}_{c=1}^C$. The weighting matrices $\mathbf{G}$ are chosen to be within a constraint set $\mathcal{G}$ of matrices. The set $\mathcal{G}$ is defined in practice to have certain desirable properties in order to facilitate implementation and control the complexity of our framework. We consider the following optimization problem:

$$\min_{\mathbf{G} \in \mathcal{G}, w_p \in \mathcal{H}} \frac{1}{N} \sum_{i=1}^{N} \phi(p_i \langle w_p, \Phi(\mathbf{Z}_i) \rangle) + \frac{\lambda_p}{2} \|w_p\|^2, \tag{3a}$$

$$\text{s.t.} \min_{w_q \in \mathcal{H}} R(\mathbf{G}, w_q) \geq \theta, \tag{3b}$$

where $w_p$ and $w_q$ are the fusion center decision rules for inferring the public and private hypotheses respectively,

$$R(\mathbf{G}, w_q) = \sum_{k \in \{-1,1\}} \frac{1}{2|\mathcal{S}_k|} \sum_{i \in \mathcal{S}_k} \phi(q_i \langle w_q, \Phi(\mathbf{Z}_i) \rangle) + \frac{\lambda_q}{2} \|w_q\|^2, \tag{4}$$

$\mathcal{S}_k = \{1 \leq i \leq N : q_i = k\}$, and $\theta$ is called the privacy threshold. The regularization weights $\lambda_p$ and $\lambda_q$ are small positive constants. We call (4) the *empirical normalized risk*, since unlike the traditional empirical risk (of which (3a) is an example), we now have a normalization term $|\mathcal{S}_k|$ in (4). It turns out that this normalization term plays a critical role in achieving information privacy as one can construct examples in which using the traditional empirical risk without the normalization term fails to achieve $(\epsilon, \delta)$-information privacy for any given $\epsilon > 0$ and $\delta \in (0, 1)$ [34]. We need the following assumption.

**Assumption 2.** *For any $w \in \mathcal{H}$, there exists $\alpha_k \in \mathbb{R}$, $b_k \in \mathbb{R}$ and $\mathbf{r}_k \in \mathbb{R}^{dkC}$, for $k \geq 1$, such that for all $\mathbf{Z} \in \mathbb{U}$,*

$$w(\mathbf{Z}) = \sum_{k \geq 1} \alpha_k v(\mathbf{Z}) u(\mathbf{r}_k^T \mathbf{Z} + b_k),$$

*where $v(\cdot)$ is a positive continuous function, and $u(\cdot)$ is a nonpolynomial continuous function.*

An example of a kernel inducing a RKHS $\mathcal{H}$ satisfying Assumption 2 is the Gaussian kernel. We have the following result, similar to Theorem 2 of [34], which applies to the commonly used loss functions shown in Table II of [34].

**Theorem 1.** *Suppose that Assumption 1 and Assumption 2 hold. Suppose that the loss function $\phi(\cdot)$ is either an exponential, logistic, hinge or quadratic loss. Suppose also that $\lambda_q \to 0$ as the number of training samples $n \to \infty$. Then, for any $\delta \in (0, 1)$, there exist $\xi > 0$, and $N_0 > 0$ such that if $N \geq N_0$, the constraint* (3b) *achieves $(\epsilon, \delta)$-information privacy with $\epsilon = \log \frac{\xi}{\left(\xi - 2a(\phi(0) - \theta + \delta')^{\frac{1}{r}}\right)_+}$, where $\delta' = \min\{\xi^{2r}/2a, \delta/2\}$, and $a$ and $r$ are constants associated with the loss function $\phi$ shown in Table II of [34].*

*Proof:* See Appendix A. ∎

Theorem 1 shows that by using a sufficiently large number of training samples and choosing $\theta$ sufficiently close to $\phi(0)$, we can make $\epsilon \to 0$ and $\delta \to 0$, i.e., achieve arbitrarily strong information privacy. However, stronger information privacy leads to a higher error rate for the public hypothesis $p$. In the following section, to control the trade-off between privacy protection and public information detection, we propose model restrictions on the weighting matrices $\mathbf{G} = \{\mathbf{G}^c\}_{c=1}^C$ , and an algorithm to determine the best privacy threshold $\theta$ and mapping $\mathbf{Z}(\cdot)$ to use.

## III. Model restrictions and Algorithm Design

In this section, we first propose an algorithm to solve the optimization problem (3). Then, we introduce model restrictions in the form of constraints for the weighting matrices $\mathbf{G} = \{\mathbf{G}^c\}_{c=1}^C$. We propose a modified mirror descent approach to solve the optimization problem (3) with model restrictions, and derive the gradient updates needed for the case where the weighting matrices are positive semidefinite (PSD) with small traces.

Writing the privacy constraint (3b) in dual form, the optimization problem (3) is equivalent to

$$\min_{\mathbf{G} \in \mathcal{G}, w_p} \frac{1}{N} \sum_{i=1}^{N} \phi(p_i \langle w_p, \Phi(\mathbf{Z}_i) \rangle) + \frac{\lambda_p}{2} \|w_p\|^2, \tag{5a}$$

$$\text{s.t.} \max_{\boldsymbol{\beta}} R^*(\mathbf{G}, \boldsymbol{\beta}) \geq \theta, \tag{5b}$$

where

$$R^*(\mathbf{G}, \boldsymbol{\beta}) = - \sum_{k \in \{-1,1\}} \frac{1}{2|\mathcal{S}_k|} \sum_{i \in \mathcal{S}_k} \phi^*(-2|\mathcal{S}_k| \boldsymbol{\beta}(i)) - \frac{1}{2\lambda_q} (\mathbf{q} \circ \boldsymbol{\beta})^T \mathbf{K}(\mathbf{G}, \overline{\mathbf{X}}) (\mathbf{q} \circ \boldsymbol{\beta}), \tag{6}$$

$\mathbf{p} = (p_i)_{i=1}^n$, $\mathbf{q} = (q_i)_{i=1}^n$, $\overline{\mathbf{X}} = \{\mathbf{X}_i\}_{i=1}^n$, and the $(i, j)$-th element of the kernel matrix $\mathbf{K}(\mathbf{G}, \overline{\mathbf{X}})$ is $\kappa(\mathbf{Z}_i, \mathbf{Z}_j)$. The function $\phi^*(\cdot)$ is the conjugate dual of $\phi(\cdot)$.

We derive algorithms to first find an appropriate privacy threshold $\theta$ and then to solve (5) for the optimal $\mathbf{G}$. Since the optimization problem (5) is non-convex and the problem dimension is generally large, we adopt a gradient descent approach in both algorithms.

1) *Finding the threshold $\theta$:* The gradient of $R^*(\mathbf{G}, \boldsymbol{\beta})$ in (6) with respect to (w.r.t.) $\mathbf{G}_m^c$ can be shown to be

$$\mathbf{g}_m^c(\mathbf{G}^c, \boldsymbol{\beta}; \mathbf{q}, \lambda_q) = - \frac{1}{2\lambda_q} \sum_{i=1}^{N} \sum_{j=1}^{N} \boldsymbol{\beta}(i) \boldsymbol{\beta}(j) q_i q_j \frac{\partial \kappa(\mathbf{Z}_i, \mathbf{Z}_j)}{\partial \mathbf{G}_m^c}, \tag{7}$$

where an example of how to compute the gradient $\partial\kappa(\mathbf{Z}_i, \mathbf{Z}_j)/\partial\mathbf{G}_m^c$ for the Gaussian kernel is presented in Section IV-A. With the gradient in (7), we use an iterative gradient-based method to solve

$$\max_{\mathbf{G}\in\mathcal{G},\boldsymbol{\beta}} R^*(\mathbf{G}, \boldsymbol{\beta}), \tag{8}$$

which gives us the empirical normalized risk of detecting the private hypothesis $q$ under the worst case $\mathbf{G}$. Let the objective value of (8) be $\theta^*$. We then choose $\theta = \zeta\theta^*$ for a fixed $\zeta \in (0, 1)$. The algorithm to find $\theta^*$ is given in Algorithm 1.

2) *Solving the optimization problem* (5)*:* The optimization problem (5) can be solved by an alternative minimization between $w_p$ and $\mathbf{G}$. With a fixed feasible $\mathbf{G}$, the minimization of the objective function in (5a) w.r.t. $w_p$ can be obtained through its dual maximization due to strong duality:

$$\max_{\boldsymbol{\alpha}} \; F^*(\mathbf{G}, \boldsymbol{\alpha}) = -\frac{1}{N}\sum_{i=1}^{N}\phi^*(-n\boldsymbol{\alpha}(i)) - \frac{1}{2\lambda_p}(\mathbf{p}\circ\boldsymbol{\alpha})^T\mathbf{K}(\mathbf{G}, \overline{\mathbf{X}})(\mathbf{p}\circ\boldsymbol{\alpha}), \tag{9}$$

which can be solved using Algorithm 2 to obtain the optimal $\boldsymbol{\alpha}$. Setting $w_p = \sum_{j=1}^{l}\boldsymbol{\alpha}(j)p_j\Phi(\mathbf{Z}_j)$, the gradient of the objective function in (5a) w.r.t. $\mathbf{G}_m^c$ can then be obtained as

$$\mathbf{g}_m^c(\mathbf{G}^c, \boldsymbol{\alpha}; \mathbf{p}, \lambda_p) = -\frac{1}{2\lambda_p}\sum_{i=1}^{N}\sum_{j=1}^{N}\boldsymbol{\alpha}(i)\boldsymbol{\alpha}(j)p_ip_j\frac{\partial\kappa(\mathbf{Z}_i, \mathbf{Z}_j)}{\partial\mathbf{G}_m^c}. \tag{10}$$

The algorithm to solve (5) without model constraints on the weighting matrices is detailed in Algorithm 3. In the following subsections, we consider the case where model constraints are now included, and propose a modified mirror descent approach.

### A. Modified Mirror Descent for Model Restrictions

We now consider adding model restrictions to the constraint set $\mathcal{G}$ to control the complexity of our multilayer nonlinear processing framework. A general way to solve the optimization problem (3) with model restrictions is the projected gradient method. However, the projected gradient method, in general, does not have a closed-form solution in each descent step, making practical implementation difficult. The mirror descent method allows for a closed-form solution at each descent step, but it is only suitable for convex problems [35]. Therefore, we develop a modified mirror descent method for our non-convex problem (3) with model restrictions. We start off with some mathematical preliminaries.

**Definition 2.** *Let $\psi(\cdot)$ be a continuous function on a given matrix space. For any matrices $\mathbf{x}$ and $\mathbf{y}$ with the appropriate dimensions, let $\langle\mathbf{x}, \mathbf{y}\rangle = \mathrm{Tr}(\mathbf{x}^T\mathbf{y})$.*

*(i) If $\|\psi(\mathbf{x}) - \psi(\mathbf{y})\| \le L\|\mathbf{x} - \mathbf{y}\|$ for all $\mathbf{x}$ and $\mathbf{y}$, we say that $\psi$ is Lipschitz continuous with Lipschitz constant $L$.*

**Algorithm 1** Finding $\theta^*$ without model restrictions.

**initialization:** initialize $\mathbf{G}[0]$ randomly and set $n = 0$.
**repeat**
  Solve the convex problem
$$\max_{\boldsymbol{\beta}} R^*(\mathbf{G}[n], \boldsymbol{\beta}) \tag{11}$$
  by Algorithm 2. Denote the optimal solution as $\boldsymbol{\beta}[n]$ and let $K[n] = R^*(\mathbf{G}[n], \boldsymbol{\beta}[n])$.
  **for** $c = 1$ to $C$ **do**
    **for** $m = M$ to $1$ **do**
      Let $\mathbf{A} = \mathbf{g}_m^c(\{\mathbf{G}_1^c[n], \ldots, \mathbf{G}_m^c[n], \mathbf{G}_{m+1}^c[n+1], \ldots, \mathbf{G}_M^c[n+1]\}, \boldsymbol{\beta}[n]; \mathbf{q}, \lambda_q)$.
      Update $\mathbf{G}_m^c[n+1] = \mathbf{G}_m^c[n] + \Delta t_m^c\mathbf{A}$, where $\Delta t_m^c$ is obtained by backtracking line search.
    **end for**
  **end for**
  Set $\mathbf{G}[n+1] = \{(\mathbf{G}_m^c[n+1])_{m=1}^M : c = 1, \ldots, C\}$, and $n = n + 1$.
**until** $(K[n+1] - K[n])/K[n] \le \epsilon$
**output:** $\theta^* = K[n+1]$.

**Algorithm 2** Maximizing $R^*(\mathbf{G}, \boldsymbol{\beta})$ or $F^*(\mathbf{G}, \boldsymbol{\beta})$ for fixed $\mathbf{G}$.

Let $K(\boldsymbol{\beta}) = R^*(\mathbf{G}, \boldsymbol{\beta})$ or $F^*(\mathbf{G}, \boldsymbol{\beta})$.
**initialization:** Initialize $\boldsymbol{\beta}[0] = \mathbf{0}$, $\rho \in (0, 1)$ and $n = 0$.
**repeat**
  $n = n + 1, t = t_0$.
  **repeat**
    Update $\boldsymbol{\beta}[n] = \mathcal{P}_b(\boldsymbol{\beta}[n-1] + t\nabla K(\boldsymbol{\beta}[n-1]))$, where $\mathcal{P}_b$ is the projection operator to the domain of $\phi^*$. For example, for the hinge and logistic loss functions, applying $\mathcal{P}_b$ on each component $\boldsymbol{\beta}(i)$, where $i \in \mathcal{S}_k$, we have
$$\mathcal{P}_b(\boldsymbol{\beta}(i)) = \begin{cases} 0, & \text{if } \boldsymbol{\beta}(i) < 0, \\ \beta_i, & \text{if } 0 \le \boldsymbol{\beta}(i) \le \dfrac{1}{2|\mathcal{S}_k|}, \\ \dfrac{1}{2|\mathcal{S}_k|}, & \text{if } \boldsymbol{\beta}(i) > \dfrac{1}{2|\mathcal{S}_k|}. \end{cases} \tag{12}$$
    Set $t = \rho t$.
  **until** $K(\boldsymbol{\beta}[n-1]) \le K(\boldsymbol{\beta}[n])$
**until** $(K(\boldsymbol{\beta}[n]) - K(\boldsymbol{\beta}[n-1]))/K(\boldsymbol{\beta}[n]) \le \epsilon$
**output:** $\boldsymbol{\beta}[n]$ and $K(\boldsymbol{\beta}[n])$.

*(ii) If $\psi$ is strictly convex, its Bregman distance is defined as*

$$B_\psi(\mathbf{x}, \mathbf{y}) = \psi(\mathbf{x}) - \psi(\mathbf{y}) - \langle\nabla\psi(\mathbf{y}), \mathbf{x} - \mathbf{y}\rangle, \tag{13}$$

*where $B(\mathbf{x}, \mathbf{y}) \ge 0$ and $B(\mathbf{x}, \mathbf{y}) = 0$ if and only if $\mathbf{x} = \mathbf{y}$. We say that $\psi(\mathbf{x})$ is $\delta$-strongly convex if*

$$B_\psi(\mathbf{x}, \mathbf{y}) \ge \frac{\delta}{2}\|\mathbf{x} - \mathbf{y}\|^2. \tag{14}$$

We make the following assumption in this section.

**Assumption 3.** *The gradients in* (7) *and* (10) *are Lipschitz continuous with Lipschitz constant $L$.*

**Algorithm 3** Solving (5) without model restrictions.

1: **initialization:** Set $n = 0$ and $\mathbf{G}[0]$ to be the final $\mathbf{G}[n]$ in Algorithm 1.
2: **repeat**
3: Maximize $F^*(\mathbf{G}[n], \boldsymbol{\alpha})$ in (9) using Algorithm 2, and let the optimal solution and optimal value be denoted as $\boldsymbol{\alpha}[n]$ and $K[n]$, respectively.
4: **for** $c = 1$ to $C$ **do**
5: **for** $m = M$ to 1 **do**
6: Let $\mathbf{A} = \mathbf{g}_m^c(\{\mathbf{G}_1^c[n], \ldots, \mathbf{G}_m^c[n], \mathbf{G}_{m+1}^c[n+1], \ldots, \mathbf{G}_M^c[n+1]\}, \boldsymbol{\alpha}[n]; \mathbf{p}, \lambda_p)$.
7: Update $\mathbf{G}_m^c[n+1] = \mathbf{G}_m^c[n] - \Delta t_m^c \mathbf{A}$, where $\Delta t_m^c$ is obtained by backtracking line search, which is restricted such that the objective function (5a) is decreased and the privacy constraint (5b) is satisfied.
8: **end for**
9: **end for**
10: Set $\mathbf{G}[n+1] = \{(\mathbf{G}_m^c[n+1])_{m=1}^M : c = 1, \ldots, C\}$, and $n = n + 1$.
11: **until** $(K[n] - K[n+1])/K[n] \leq \epsilon$
12: **output:** $\mathbf{G}[n+1]$.

Recall that after maximizing $F^*(\mathbf{G}, \boldsymbol{\alpha})$ over $\boldsymbol{\alpha}$ in (9), $F^*(\mathbf{G}, \boldsymbol{\alpha})$ is minimized over $\mathbf{G} \in \mathcal{G}$ in (5a). Let $J_p(\mathbf{G}_m^c) = F^*(\mathbf{G}, \boldsymbol{\alpha})$ for a fixed $\boldsymbol{\alpha}$ and $\mathbf{G} \backslash \{\mathbf{G}_m^c\}$. To minimize $J_p(\mathbf{G}_m^c)$ over $\mathbf{G}_m^c \in \mathcal{G}_m^c$, we propose an iterative procedure in Algorithm 4. Let $\mathbf{G}_m^c[n]$ be the solution in the $n$-th iteration of Algorithm 4. From Assumption 3, we have from [36],

$$J_p(\mathbf{G}_m^c) \leq J_p(\mathbf{G}_m^c[n]) + \langle \nabla J_p(\mathbf{G}_m^c[n]), \mathbf{G}_m^c - \mathbf{G}_m^c[n] \rangle + \frac{L}{2} \|\mathbf{G}_m^c - \mathbf{G}_m^c[n]\|^2. \tag{15}$$

From (14), for any given $\delta$-strongly convex $\psi$, we have for any $t_m^c \in (0, \delta/L]$,

$$J_p(\mathbf{G}_m^c) \leq J_p(\mathbf{G}_m^c[n]) + \underbrace{\langle \nabla J_p(\mathbf{G}_m^c[n]), \mathbf{G}_m^c - \mathbf{G}_m^c[n] \rangle + \frac{1}{t_m^c} B_\psi(\mathbf{G}_m^c, \mathbf{G}_m^c[n])}_{u_\psi(\mathbf{G}_m^c, \mathbf{G}_m^c[n]; t_m^c)}, \tag{16}$$

Instead of minimizing the non-convex $J_p(\mathbf{G}_m^c)$ directly, we propose to successively minimize the convex upper bound in (16) over the constraint set $\mathcal{G}_m^c$, i.e.,

$$\mathbf{G}_m^c[n+1] = \underset{\mathbf{G}_m^c \in \mathcal{G}_m^c}{\arg\min}\, u_\psi(\mathbf{G}_m^c, \mathbf{G}_m^c[n]; t_m^c). \tag{17}$$

From (16), we have

$$J_p(\mathbf{G}_m^c[n+1]) \leq J_p(\mathbf{G}_m^c[n]) + u_\psi(\mathbf{G}_m^c[n+1], \mathbf{G}_m^c[n]; t_m^c) \tag{18}$$

$$\leq J_p(\mathbf{G}_m^c[n]) + u_\psi(\mathbf{G}_m^c[n], \mathbf{G}_m^c[n]; t_m^c) \tag{19}$$

$$= J_p(\mathbf{G}_m^c[n]), \tag{20}$$

which shows that our proposed Algorithm 4 converges since $J_p(\cdot)$ is non-negative.

**Algorithm 4** Algorithm for successive convex upper bound minimization

1: **input:** $n, \mathbf{G}[n], \boldsymbol{\alpha}[n], \rho \in (0, 1)$.
2: Let $J_p(\mathbf{G}_m^c) = F^*(\{\mathbf{G}_m^c\} \cup (\mathbf{G}[n] \backslash \{\mathbf{G}_m^c[n]\}), \boldsymbol{\alpha}[n])$. Set $t_m^c = t_0$.
3: **repeat**
4: $t_m^c = \rho t_m^c$ and $\mathbf{G}_m^c[n+1] = \min_{\mathbf{G}_m^c \in \mathcal{G}_m^c} u_\psi(\mathbf{G}_m^c, \mathbf{G}_m^c[n]; t_m^c)$.
5: **until** $J_p(\mathbf{G}_m^c[n+1]) \leq J_p(\mathbf{G}_m^c[n]) + u_\psi(\mathbf{G}_m^c[n+1], \mathbf{G}_m^c[n]; t_m^c)$ or $|\mathbf{G}_m^c[n+1] - \mathbf{G}_m^c[n]| \leq \epsilon$.
6: **output:** $\mathbf{G}_m^c[n+1]$.

On the other hand, $R^*(\mathbf{G}, \boldsymbol{\beta})$ in (8) is maximized over $\mathbf{G} \in \mathcal{G}$. Let $J_q(\mathbf{G}_m^c) = R^*(\mathbf{G}, \boldsymbol{\beta})$ for a fixed $\boldsymbol{\beta}$ and $\mathbf{G} \backslash \{\mathbf{G}_m^c\}$. From Assumption 3, a concave lower bound of $J_q(\mathbf{G}_m^c)$ is obtained in Appendix B as

$$J_q(\mathbf{G}_m^c) \geq J_q(\mathbf{G}_m^c[n]) + \langle \nabla J_q(\mathbf{G}_m^c[n]), \mathbf{G}_m^c - \mathbf{G}_m^c[n] \rangle - \frac{L}{2} \|\mathbf{G}_m^c - \mathbf{G}_m^c[n]\|^2. \tag{21}$$

Again with (14) and $t_m^c \in (0, \delta/L]$, we have

$$J_q(\mathbf{G}_m^c) \geq J_q(\mathbf{G}_m^c[n]) + \underbrace{\langle \nabla J_q(\mathbf{G}_m^c[n]), \mathbf{G}_m^c - \mathbf{G}_m^c[n] \rangle - \frac{1}{t_m^c} B_\psi(\mathbf{G}_m^c, \mathbf{G}_m^c[n])}_{l_\psi(\mathbf{G}_m^c, \mathbf{G}_m^c[n]; t_m^c)}. \tag{22}$$

Similar to (16), we propose a successive concave lower bound maximization procedure to maximize $J_q(\mathbf{G}_m^c)$ over $\mathbf{G}_m^c \in \mathcal{G}_m^c$, as described in Algorithm 5.

**Algorithm 5** Algorithm for successive concave lower bound maximization

1: **input:** $n, \mathbf{G}[n], \boldsymbol{\beta}[n], \rho \in (0, 1)$.
2: Let $J_q(\mathbf{G}_m^c) = R^*(\{\mathbf{G}_m^c\} \cup (\mathbf{G}[n] \backslash \{\mathbf{G}_m^c[n]\}), \boldsymbol{\beta}[n])$. Set $t_m^c = t_0$.
3: **repeat**
4: $t_m^c = \rho t_m^c$ and $\mathbf{G}_m^c[n+1] = \max_{\mathbf{G}_m^c \in \mathcal{G}_m^c} l_\psi(\mathbf{G}_m^c, \mathbf{G}_m^c[n]; t_m^c)$.
5: **until** $J_q(\mathbf{G}_m^c[n+1]) \geq J_q(\mathbf{G}_m^c[n]) + l_\psi(\mathbf{G}_m^c[n+1], \mathbf{G}_m^c[n]; t_m^c)$ or $|\mathbf{G}_m^c[n+1] - \mathbf{G}_m^c[n]| \leq \epsilon$.
6: **output:** $\mathbf{G}_m^c[n+1]$.

By using the Bergman divergence, we have transformed a nonconvex optimization problem into a series of convex optimization subproblems, which allow us to adapt Algorithms 1 and 3 when model constraints are imposed on $\mathcal{G}$. We first choose a $\delta$-strongly convex function $\psi$, and then in Algorithm 1 and Algorithm 3, we update $\mathbf{G}_m^c[n+1]$ by replacing lines 6 and 7 with Algorithm 5 and Algorithm 4, respectively. In the next subsection, we provide a specific example for illustration.

### *B. PSD Weighting Constraint*

As an example, we now consider the case where the weighting matrices are PSD. Together with the trace restriction

$\mathrm{Tr}(\mathbf{G}_m^c) \leq r_m^c$, i.e., $\mathcal{G}_m^c = \{\mathbf{G}_m^c \succeq 0, \mathrm{Tr}(\mathbf{G}_m^c) \leq r_m^c\}$, for $m = 1, \ldots, M$ and $c = 1, \ldots, C$. We derive closed form expressions for line 4 of Algorithms 4 and 5 in this example.

Let $\psi(\mathbf{H}) = \sum_{j=1}^d \lambda_j(\mathbf{H}) \ln(\lambda_j(\mathbf{H}))$ with $\lambda_j(\cdot)$ representing the $j$-th eigenvalue of its argument. Note that the negative entropy function $\psi(\cdot)$ is a 1-strongly convex function [35]. The minimization in line 4 of Algorithm 4 is given by

$$\min_{\mathbf{H} \in \mathcal{G}_m^c} \langle \nabla J_p(\mathbf{G}_m^c[n]), \mathbf{H} - \mathbf{G}_m^c[n] \rangle + \frac{1}{t_m^c} B_\psi(\mathbf{H}, \mathbf{G}_m^c[n]). \tag{23}$$

To avoid numerical errors that make the computed gradient non-symmetric, we apply a symmetric projection $\mathcal{P}\left(\nabla J_p(\mathbf{G}_m^c[n])\right) = (\nabla J_p(\mathbf{G}_m^c[n]) + \nabla J_p(\mathbf{G}_m^c[n])^T)/2$, which is the optimal solution of $\min_{\mathbf{Y}=\mathbf{Y}^T} \|\mathbf{Y} - \nabla J_p(\mathbf{G}_m^c[n])\|_F^2$, and replace $\nabla J_p(\mathbf{G}_m^c[n])$ in (23) with $\mathcal{P}(\nabla J_p(\mathbf{G}_m^c[n]))$. Simplifying (23), we have

$$\min_{\mathbf{H} \in \mathcal{G}_m^c} \langle \mathcal{P}\left(\nabla J_p(\mathbf{G}_m^c[n])\right) - \frac{1}{t_m^c} \nabla \psi(\mathbf{G}_m^c[n]), \mathbf{H} \rangle + \frac{1}{t_m^c} \sum_{j=1}^d \lambda_j(\mathbf{H}) \ln(\lambda_j(\mathbf{H})), \tag{24}$$

where $\nabla \psi(\mathbf{G}_m^c[n]) = \sum_{j=1}^d (\ln(\lambda_j(\mathbf{G}_m^c[n])) + 1) \mathbf{u}_j \mathbf{u}_j^T$, and $\mathbf{u}_j$ is the $j$-th eigenvector of the matrix $\mathbf{G}_m^c[n]$. The closed form solution of (24) is given in the following result.

**Proposition 1.** *The optimal solution of* (24) *is* $\mathbf{H} = \mathbf{U}\mathrm{Diag}(\lambda(\mathbf{H}))\mathbf{U}^T$, *where* $\mathbf{U}$ *comes from the eigendecomposition of* $\mathcal{P}\left(\nabla J_p(\mathbf{G}_m^c[n])\right) - \frac{1}{t_m^c} \nabla \psi(\mathbf{G}_m^c[n]) = \mathbf{U}\mathrm{Diag}([\sigma_1, \cdots, \sigma_d])\mathbf{U}^T$, *and the eigenvalues are obtained as*

$$\lambda_j(\mathbf{H}) = \begin{cases} \exp(-\sigma_j t_m^c - 1), & \text{if } \sum_{j=1}^d \exp(-\sigma_j t_m^c - 1) < r_m^c; \\ \frac{r_m^c \exp(-\sigma_j t_m^c - 1)}{\sum_{j=1}^d \exp(-\sigma_j t_m^c - 1)}, & \text{otherwise.} \end{cases} \tag{25}$$

*Proof.* Since the symmetric matrix can be factorized as $\mathbf{H} = \mathbf{U}\mathrm{Diag}(\lambda(\mathbf{H}))\mathbf{U}^T$, it is obvious that the eigenvectors of the optimal solution in $\min_{\mathbf{H} \in \mathcal{G}_m^c} \langle \mathcal{P}\left(\nabla J_p(\mathbf{G}_m^c[n])\right) - \frac{1}{t_m^c} \nabla \psi(\mathbf{G}_m^c[n]), \mathbf{H} \rangle$ are the eigenvectors of $\mathcal{P}\left(\nabla J_p(\mathbf{G}_m^c[n])\right) - \frac{1}{t_m^c} \nabla \psi(\mathbf{G}_m^c[n]) = \mathbf{U}\mathrm{Diag}([\sigma_1, \cdots, \sigma_d])\mathbf{U}^T$. Therefore, the problem (24) is equivalent to

$$\begin{aligned} \min_{\{\lambda_j(\mathbf{H})\}_{j=1}^d} \; & \sum_{j=1}^d \lambda_j(\mathbf{H}) \sigma_j + \frac{1}{t_m^c} \sum_{j=1}^d \lambda_j(\mathbf{H}) \ln(\lambda_j(\mathbf{H})) \\ \text{s.t.} \; & \sum_{j=1}^d \lambda_j(\mathbf{H}) \leq r_m^c, \\ & \lambda_j(\mathbf{H}) \geq 0, \text{for } j = 1, \ldots, d. \end{aligned} \tag{26}$$

With Lagrange multipliers $\mu$ and $\{\nu_j\}_{j=1}^d$, the Lagrangian of (26) is

$$\mathcal{L} = \sum_{j=1}^d \lambda_j(\mathbf{H}) \sigma_j + \frac{1}{t_m^c} \sum_{j=1}^d \lambda_j(\mathbf{H}) \ln(\lambda_j(\mathbf{H})) + \mu(\sum_{j=1}^d \lambda_j(\mathbf{H}) - r_m^c) - \sum_{j=1}^d \nu_j \lambda_j(\mathbf{H}). \tag{27}$$

Letting $\frac{\partial \mathcal{L}}{\partial \lambda_j(\mathbf{H})} = 0$, we obtain the condition $\lambda_j(\mathbf{H}) = \exp((\nu_j - \mu) t_m^c) \exp(-\sigma_j t_m^c - 1)$. Since the problem (26) is a convex problem, the optimal solution can be derived from the K.K.T. conditions:

$$\{\lambda_j(\mathbf{H}) = \exp((\nu_j - \mu) t_m^c) \exp(-\sigma_j t_m^c - 1)\}_{j=1}^d \tag{28}$$

$$\sum_{j=1}^d \lambda_j(\mathbf{H}) \leq r_m^c \tag{29}$$

$$\mu \geq 0, \{\nu_j \geq 0\}_{j=1}^d \tag{30}$$

$$\mu(\sum_{j=1}^d \lambda_j(\mathbf{H}) - r_m^c) = 0, \{\nu_j \lambda_j(\mathbf{H}) = 0\}_{j=1}^d. \tag{31}$$

From (28), we have $\lambda_j(\mathbf{H}) > 0$, and (31) shows that $\nu_j = 0$ for $j = 1, \cdots, d$.

When strict inequality holds in condition (29), we obtain from (31) that $\mu = 0$, and $\sum_{j=1}^d \exp(-\sigma_j t_m^c - 1) < r_m^c$. Therefore, the first case of (25) is proved.

When equality in (29) holds, we have from (31) that $\mu \geq 0$, and $\sum_{j=1}^d \exp(-\sigma_j t_m^c - 1) \geq r_m^c$. Furthermore, $\sum_{j=1}^d \lambda_j(\mathbf{H}) = r_m^c$ also leads to $\exp(-\mu t_m^c) = r_m^c / \sum_{j=1}^d \exp(-\sigma_j t_m^c - 1)$. Therefore, the second case of (25) is prove. The proof of the proposition is now complete. □

Since the maximization problem in line 4 of Algorithm 5 can be transformed into a minimization problem, it can be solved using a result similar to Proposition 1.

## IV. Experimental Evaluation

In this section, we verify the performance of our proposed approach using three real datasets: the OPPORTUNITY activity recognition dataset [37], human action recognition dataset [38], and a dataset consisting of images of guns and/or cash, which we have collected and made available at [39]. For ease of reference, we call our approach the multilayer nonlinear privacy transformation (MNPT).

To test the effectiveness of MNPT in sanitizing the sensor information, we try different learning machine techniques on the sanitized information in order to learn the private hypothesis. In our experiments, we use a support vector machine (SVM) [31], a convolutional neural network (CNN) [40], and the softmax classifier with cross entropy cost function [41]. The regularization parameter $\lambda_q$ in the SVM is tuned from $[10^{-3}, 10^2]$, and the CNN we use is the classic LeNet [40] with 32, 64, and 1024 features in the first, second convolution layer, and fully connected layer, respectively. As traditional machine learning algorithms do not perform well on our image dataset, we also implemented a residual neural network (ResNet) [42], which is a state-of-the-art deep learning technique for image recognition. Our ResNet has 44 layers, with initial learning rate 0.05, which is divided by 10 at the 300-th and 400-th iterations, and the training is terminated at 500 iterations. The LeNet and ResNet are trained with a mini-batch size of 100.

We compare with the RUCA approach proposed by [25]. Note that in our proposed MNPT approach, finding the optimal precoders $\mathbf{G}$ is done offline using a set of training data. However, during the online execution of our privacy framework, each sensor utilizes its own local linear precoder found in the offline optimization phase to transform its local observation independently of the other sensors. This is in contrast to the RUCA approach, which requires that all sensors send their

local observations to a trusted curator that then performs a privacy mapping on the aggregated data.

### A. Implementation Details

Recall that in our proposed MNPT architecture, each sensor applies a nonlinear fusion function $h : \mathbb{R}^{d\times k} \to \mathbb{R}^{d\times k}$, which operates element-wise on its input argument, to the information it receives from sensors in the previous layer. Abusing notation, we use the same symbol $h(\cdot)$ to denote the element-wise operator $\mathbb{R} \to \mathbb{R}$. We consider four choices for the nonlinear function $h(\cdot)$:

(i) logistic function $h(x) = \frac{1}{1+e^{-x}}$,
(ii) tanh function $h(x) = \frac{2}{1+e^{-2x}} - 1$,
(iii) rectified linear unit (RLU) function $h(x) = \max(0, x)$, and
(iv) sin function $h(x) = \sin(x)$.

Recall that $\mathbf{Z}_i = \mathbf{Z}(\mathbf{X}_i) = [\mathbf{Z}^1(\mathbf{G}^1, \mathbf{X}_i^1); \ldots; \mathbf{Z}^C(\mathbf{G}^C, \mathbf{X}_i^C)]$, where $\mathbf{X}_i$ is the $i$-th training sample. To avoid cluttered notations, we let $\mathbf{Z}_i^c = \mathbf{Z}^c(\mathbf{G}^c, \mathbf{X}_i^c)$ for $c = 1, \ldots, C$. We utilize the hinge loss function for $\phi$ and the Gaussian kernel $\kappa(\mathbf{Z}_i, \mathbf{Z}_j) = \exp(-\gamma\|\mathbf{Z}_i - \mathbf{Z}_j\|_F^2)$. We have

$$\frac{\partial\kappa(\mathbf{Z}_i, \mathbf{Z}_j)}{\partial\mathbf{G}_m^c} = -2\gamma\exp(-\gamma\|\mathbf{Z}_i - \mathbf{Z}_j\|_F^2)\mathbf{D}_m^c, \tag{32}$$

where for $2 \le m \le M-1$,

$$\mathbf{D}_m^c = \mathbf{B}_m^c(i,j)\mathbf{F}_{m-1}^c(\mathbf{X}_i^c) + \mathbf{B}_m^c(j,i)\mathbf{F}_{m-1}^c(\mathbf{X}_j^c), \tag{33}$$
$$\mathbf{D}_1^c = \mathbf{B}_1^c(i,j)\cdot[\mathbf{X}_i^c]^T + \mathbf{B}_1^c(j,i)\cdot[\mathbf{X}_j^c]^T, \tag{34}$$
$$\mathbf{D}_M^c = (\mathbf{Z}_i^c - \mathbf{Z}_j^c)[\mathbf{F}_{M-1}^c(\mathbf{X}_i^c) - \mathbf{F}_{M-1}^c(\mathbf{X}_j^c)], \tag{35}$$

with

$$\mathbf{F}_m^c(\mathbf{X}_i^c) = [h(\mathbf{G}_m^c \cdots h(\mathbf{G}_1^c\mathbf{X}_i^c))]^T, \tag{36}$$
$$\mathbf{B}_m^c(i,j) = \mathbf{I}_m^c(i) \circ ((\mathbf{G}_{m+1}^c)^T \cdots [\mathbf{I}_{M-1}^c(i) \circ ((\mathbf{G}_M^c)^T (\mathbf{Z}_i^c - \mathbf{Z}_j^c))]), \tag{37}$$

and

$$\mathbf{I}_m^c(i) = \begin{cases} h(\mathbf{G}_m^c \cdots h(\mathbf{G}_1^c\mathbf{X}_i^c)) \circ (1 - h(\mathbf{G}_m^c \cdots h(\mathbf{G}_1^c\mathbf{X}_i^c))), \\ \quad \text{if } h(\cdot) \text{ is the logistic function;} \\ 1 - h(\mathbf{G}_m^c \cdots h(\mathbf{G}_1^c\mathbf{X}_i^c)) \circ h(\mathbf{G}_m^c \cdots h(\mathbf{G}_1^c\mathbf{X}_i^c))), \\ \quad \text{if } h(\cdot) \text{ is the tanh function;} \\ \mathbf{1}_{\{h(\mathbf{G}_m^c \cdots h(\mathbf{G}_1^c\mathbf{X}_i^c))>0\}}, \quad \text{if } h(\cdot) \text{ is the RLU function;} \\ \cos(\mathbf{G}_m^c \cdots h(\mathbf{G}_1^c\mathbf{X}_i^c)), \quad \text{if } h(\cdot) \text{ is the sin function;} \end{cases}$$

where $\mathbf{1}_{\{\cdot\}}$ operates element-wise on its input matrix. The gradient in Algorithm 2 when $K(\boldsymbol{\beta}) = R^*(\mathbf{G}, \boldsymbol{\beta})$ can be shown to be

$$\nabla K(\boldsymbol{\beta}) = -1 - \frac{1}{\lambda_q}\mathrm{Diag}(\mathbf{q})\mathbf{K}(\mathbf{G}, \overline{\mathbf{X}})\mathrm{Diag}(\mathbf{q})\boldsymbol{\beta}. \tag{38}$$

A similar expression can be obtained for the case where $K(\boldsymbol{\beta}) = F^*(\mathbf{G}, \boldsymbol{\beta})$.

We impose the trace restriction $\{\{\mathrm{Tr}(\mathbf{G}_m^c) \le r_m^c = 1\}_{m=1}^M\}_{c=1}^C$, as discussed in Section III-B. In Algorithm 5, the weighting matrices $\{\{\mathbf{G}_m^c[0]\}_{m=1}^M\}_{c=1}^C$ are initialized as normalized identity matrices. We choose the Gaussian kernel parameter $\gamma$ to be the inverse of the median of the set $\{\sum_{c=1}^C \|\mathbf{Z}_i^c - \mathbf{Z}_j^c\|^2 : i, j \in [1, l], i \ne j\}$, the termination threshold $\epsilon = 10^{-3}$, the initial step size $t_0 = 1$, and the factor $\rho = 0.8$.

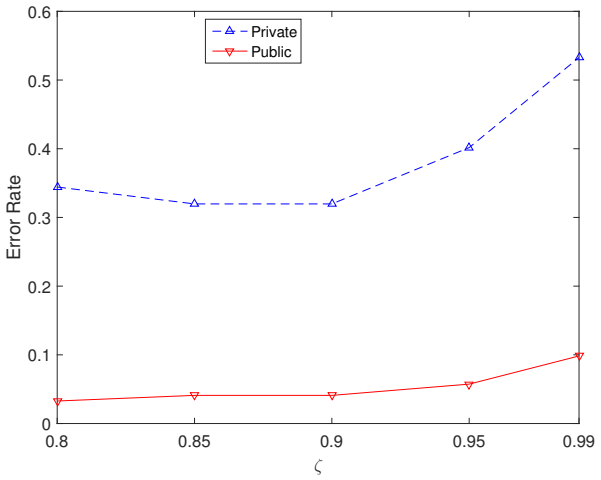


Fig. 5. MNPT for OPPORTUNITY activity recognition with $M = 2$: The impact of the parameter $\zeta$ on the public and private hypothesis error rates.

### B. OPPORTUNITY Activity Recognition

We test our algorithm on the OPPORTUNITY activity recognition dataset in [37]. The public hypothesis is to detect whether a person opens or closes a door, and the private hypothesis is to detect whether he is walking or standing. The data in columns 64 to 76 (left arm's sensor), columns 103 to 134 (shoes' sensors), and that in columns 208 to 210 (door's sensor) of "S2-Drill", over a time horizon of 20 samples is taken as $\mathbf{X} \in \mathbb{R}^{48\times 20}$. The training sample size is $N = 50$, the testing sample size is 122, and the regularization parameters are $[\lambda_p, \lambda_q] = [0.1, 0.1]$.

In Fig. 5, the public and private hypothesis error rates with different values of $\zeta$ used to define the privacy threshold $\theta$ (cf. Section III) are shown for the case where the network has $M = 2$ layer. Fig. 5 shows that both public and private hypothesis error rates increases as $\zeta$ increases, but the error rate of the private hypothesis increases faster than that of the public hypothesis. In practice, we usually set $\zeta$ close to 1 to make the private hypothesis difficult to be detected. In our following experiments, we set $\zeta = 0.99$.

In Fig. 6, we show how the choice of the nonlinear function $h(\cdot)$ affects the detection performance. We see that the largest gap between the public and private hypothesis error rates is obtained under the RLU function. A plausible reason is that the RLU function induces sparsity in the transformed data and does not saturate [43]. In the rest of our experiments, we adopt the RLU function as $h(\cdot)$.

We next investigate how the error rates vary with the number of layers $M$. Fig. 7(a) shows that the biggest gap between the public and private hypothesis error rates occurs at $M = 3$. In this dataset, it turns out that the architecture with a larger number of layers overfits the training data, leading to a worse performance on the testing set. However, we will see that in the subsequent examples that in general a larger number of

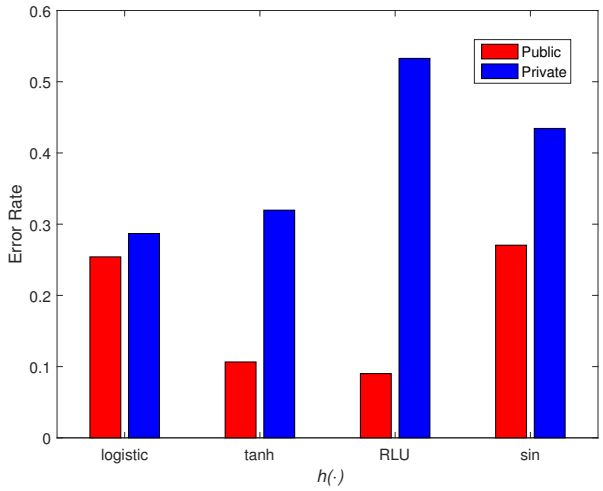


Fig. 6. MNPT for OPPORTUNITY activity recognition with $M = 3$: Different choices for $h(\cdot)$.

layers leads to better performance. This example also shows that in practice, to achieve the best performance, one should tune the number of layers using the sample dataset.

We next try different learning machine techniques on the sanitized information. From Fig. 7(b), we see that the private hypothesis error rates under different learning techniques on the sanitized information are all higher than that when performed on the raw sensor observations, which is depicted as having zero number of layers. This shows that our MNPT sanitization approach makes it difficult for these commonly used learning techniques to infer the private hypothesis.

TABLE I
RUCA FOR OPPORTUNITY ACTIVITY RECOGNITION.

| RUCA parameter $\rho_p$ | $10^{-2}$ | $10^{-1}$ | $10^{0}$ | $10^{1}$ | $10^{2}$ |
|---|---|---|---|---|---|
| Public error rate (%) | 16.39 | 13.11 | 14.75 | 15.57 | 15.57 |
| Private error rate (%) | 40.16 | 37.70 | 39.34 | 38.52 | 37.70 |

Finally, we compare our approach with $M = 3$ to RUCA, whose performance under different parameters is listed in Table I. Although the best private hypothesis error rate of RUCA at $40.16\%$ is similar to our approach, which achieves $53.28\%$, the public hypothesis error rate of RUCA is larger than that achieved by our method. We see that by using more layers, we can achieve better performance.

### C. Human Action Recognition

We test our algorithm on the multimodal dataset for human action recognition in [38]. Actions are recorded using inertial sensors and a Kinect camera. The measurements are made when the person is engaging in one of the following four activities: boxing, bowling, baseball and tennis swing. The public hypothesis is to detect whether a person is boxing or not, and the private hypothesis is to detect whether the person is playing baseball or not.

In our first experiment, we consider only data from 6 inertial sensors. We sample 132 inertial measurements uniformly from the sensors over a time period of three seconds. Each sensor

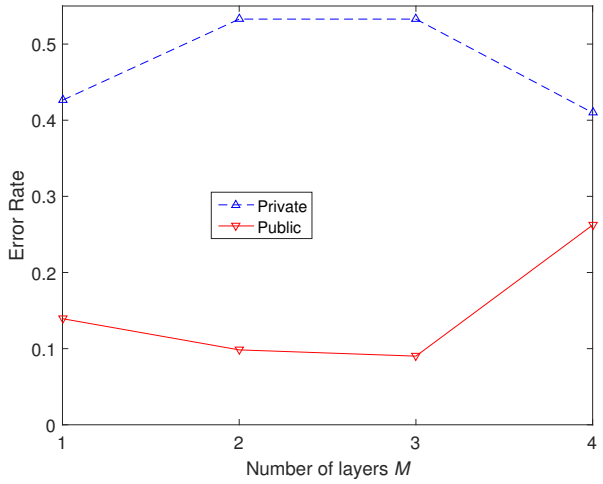


(a) The impact of the number of layers $M$ on public and private hypothesis error rates.

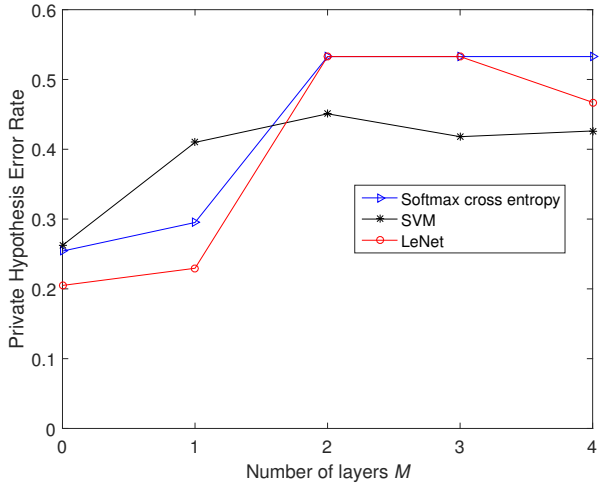


(b) The private hypothesis error rate under different learning techniques. Zero layer indicates that the learning is applied on the raw sensor observations.

Fig. 7. MNPT for OPPORTUNITY activity recognition.

forms a cluster by itself, with $\mathbf{X}^c \in \mathbb{R}^{132}$ for $c = 1, \ldots, 6$. Every sensor uses the same precoders. The training sample size is $N = 50$, testing sample size is 78, the regularization parameters are $[\lambda_p, \lambda_q] = [0.1, 0.01]$, and the parameter $\zeta = 0.9$. From Fig. 8(a), we see that the biggest gap between the public and private hypothesis error rates occurs when $M = 4$. Note that in this experiment, a random guess gives an error rate of $25\%$ since the person may be engaging in any one of the four activities.

We next compare the private hypothesis error rates under different learning techniques. From Fig. 8(b), we see that when applied to the raw sensor observations (zero layer), the private hypothesis error rates under all techniques are close to zero, while those for the sanitized information are all above $20\%$, and reaching close to $25\%$ when $M = 4$.

In our next experiment, we include data from the Kinect camera in addition to the observations from the inertial sensors. 60 coordinates on the human body, modeled as a skeleton,

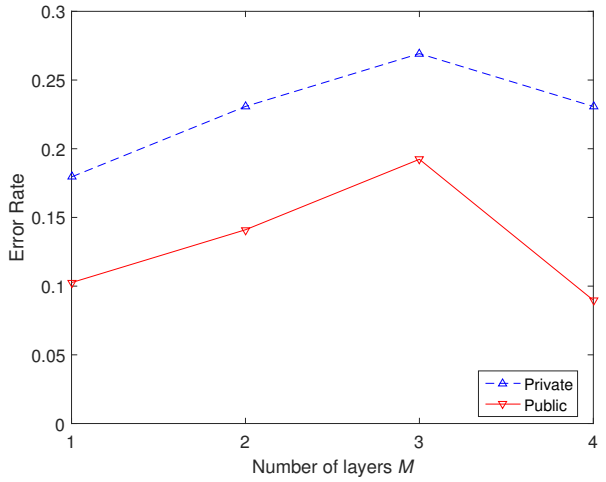


(a) The impact of the number of layers $M$ on public and private hypothesis error rates.

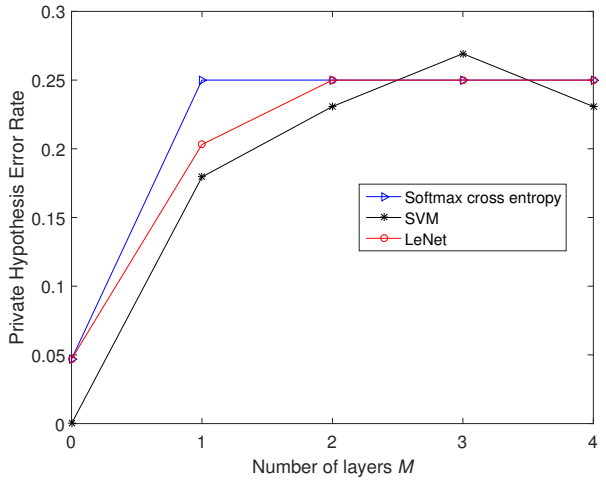


(b) The private hypothesis error rate under different learning techniques. Zero layer indicates that the learning is applied on the raw sensor observations.

Fig. 8. MNPT for human action recognition using inertial sensors.

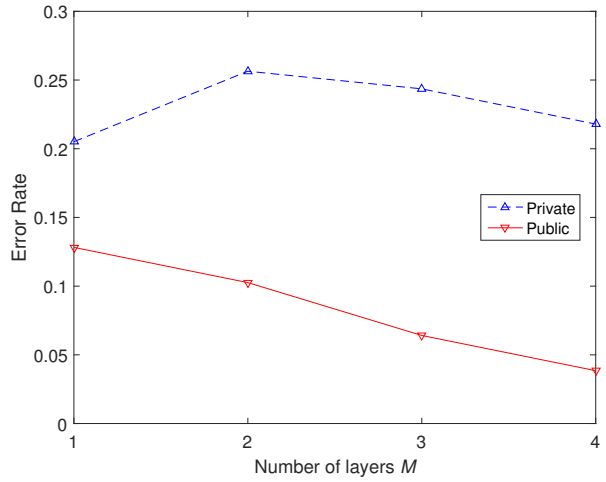


(a) The impact of the number of layers $M$ on public and private hypothesis test.

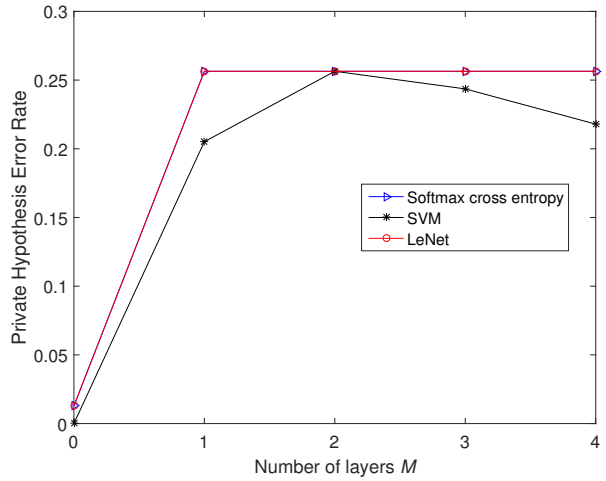


(b) The private hypothesis error rate under different learning techniques. Zero layer indicates that the learning is applied on the raw sensor observations.

Fig. 9. MNPT for human action recognition using both inertial sensors and a Kinect camera.

are tracked and 44 data points are uniformly sampled from each coordinate's trajectory, i.e., the 7-th cluster observation is formed as $\mathbf{X}^7 \in \mathbb{R}^{60\times 44}$. We set the parameter $\lambda_p = 0.01$, and other parameters are the same as the previous experiment using only inertial sensors. Compared with Fig. 8(a), Fig. 9(a) shows that at $M = 4$, a bigger gap between the public and private hypothesis error rates is achieved. This is because the data from the Kinect camera adds diversity to the available information. The sanitized information is also robust against various learning techniques as shown in Fig. 9(b).

TABLE II
RUCA FOR HUMAN ACTION RECOGNITION USING BOTH INERTIAL SENSORS AND A KINECT CAMERA.

| RUCA parameter $\rho_p$ | $10^{-2}$ | $10^{-1}$ | $10^{0}$ | $10^{1}$ | $10^{2}$ |
|---|---|---|---|---|---|
| Public error rate (%) | 7.69 | 8.97 | 8.97 | 8.97 | 8.97 |
| Private error rate (%) | 29.49 | 19.23 | 19.23 | 19.23 | 17.95 |

In Table II, we see that the private hypothesis error rates achieved by RUCA are comparable with that for MNPT with $M = 4$. However, MNPT's public hypothesis error rate is around 4%, which is much lower than those for RUCA.

### D. Gun and Cash Images

In our last set of experiments, we use a webcam to record images, which depict a gun and/or cash (dollar notes). See Fig. 10 for an example. The presence or absence of a gun is the public hypothesis, and the presence or absence of cash is the private hypothesis. The gun and the cash are randomly translated and rotated in each $80 \times 80$ grayscale image. The regularization parameters are tuned to be $[\lambda_p, \lambda_q] = [0.01, 0.1]$, and the parameter $\zeta = 0.98$. We use $N = 100$ training samples and 100 test samples.

We first test the case where if a gun is present, the same type of gun is always depicted in the image. From Fig. 11(a), we observe that the largest gap between the public and private hypothesis error rates occurs when $M = 4$, with the private

Fig. 10. Gun and cash image experiment. The presence or absence of a gun and cash are the public and private hypothesis, respectively.

hypothesis error rate being $45\%$, which is close to the error rate of $50\%$ for random guessing. In Fig. 11(b), we use various machine learning techniques to detect the private hypothesis from the sanitized information. It can be observed that SVM, softmax and LeNet do not perform well even on the unsanitized information (shown as zero number of layers in Fig. 11(b)) as these methods are not specialized for image recognition. We therefore include the ResNet here for comparison. We see that ResNet achieves a low error rate of $14\%$ compared to an error rate of $47\%$ when we use MNPT with $M = 4$.

TABLE III
RUCA FOR IMAGES WITH ONE TYPE OF GUN AND CASH.

| RUCA parameter $\rho_p$ | $10^{-2}$ | $10^{-1}$ | $10^{0}$ | $10^{1}$ | $10^{2}$ |
|---|---|---|---|---|---|
| Public error rate (%) | 32.00 | 32.00 | 32.00 | 32.00 | 32.00 |
| Private error rate (%) | 51.00 | 47.00 | 44.00 | 44.00 | 44.00 |

In Table III, the largest private hypothesis error rate of RUCA is close to that of MNPT with $M = 4$. However, for the public hypothesis, MNPT achieves an error rate of $5\%$, which is much smaller than the $32\%$ achieved by RUCA. This shows that MNPT is able to achieve a better trade-off between the public and private hypothesis error rates for this dataset.

In our next experiment, we use a dataset in which if a gun is present, then it can be one of three different types of guns. The regularization parameters are tuned to be $[\lambda_p, \lambda_q] = [0.01, 0.01]$, and the parameter $\zeta = 0.999$. We use $N = 300$ training samples and 300 testing samples. Fig. 12(a) shows that $M = 5$ provides the best trade-off between public hypothesis detection and protection of the private hypothesis. Furthermore, Fig. 12(b) shows that, under different learning techniques, the private hypothesis error rates of the sanitized images are higher than those for the raw images.

TABLE IV
RUCA FOR IMAGES WITH THREE TYPES OF GUN AND CASH.

| RUCA parameter $\rho_p$ | $10^{-2}$ | $10^{-1}$ | $10^{0}$ | $10^{1}$ | $10^{2}$ |
|---|---|---|---|---|---|
| Public error rate (%) | 32.67 | 32.00 | 31.67 | 31.67 | 31.67 |
| Private error rate (%) | 55.33 | 52.67 | 52.33 | 51.67 | 51.67 |

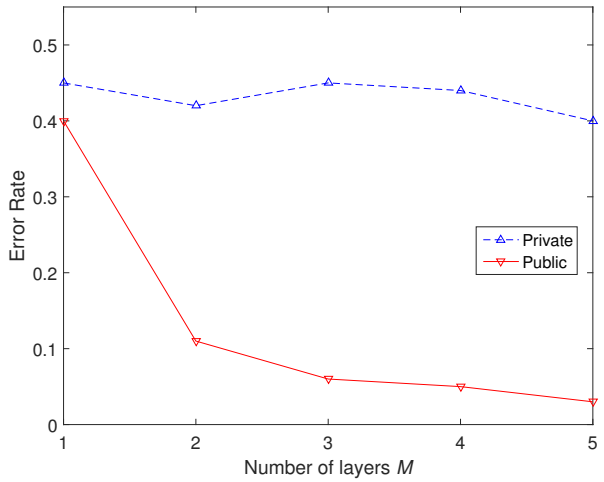


(a) The impact of the number of layers $M$ on public and private hypothesis test.

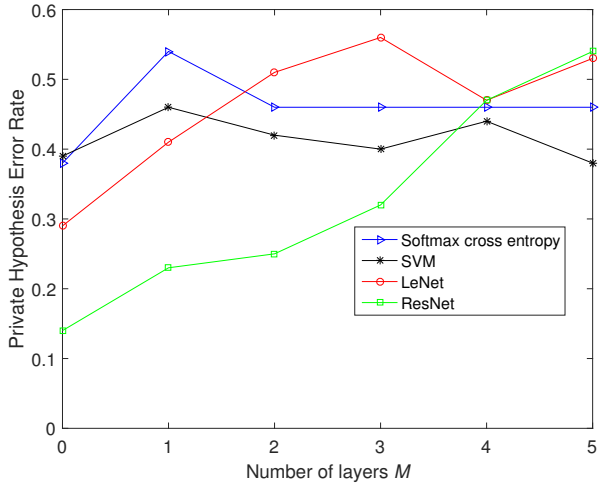


(b) The private hypothesis error rate under different learning techniques. Zero layer indicates that the learning is applied on the raw sensor observations.

Fig. 11. MNPT for images with one type of gun and cash.

We see from Table IV that the largest private hypothesis error rate of RUCA is close to that of MNPT with $M = 5$. However, for the public hypothesis, MNPT achieves a much smaller error rate than RUCA.

## V. CONCLUSION

We have proposed a multilayer nonlinear processing framework to design practical privacy mappings at each sensor in an IoT network in order to sanitize information related to a private hypothesis while enabling the fusion center to still infer a public hypothesis based on the sanitized information. Our approach involves performing a non-linear mapping, followed by a linear weighting on the information received by each sensor, which is inspired by techniques used in the neural network literature. To optimize the linear weighting matrices, we proposed an empirical risk minimization approach so that these weights can be learned from a set of training data. We developed a modified mirror descent method to solve the

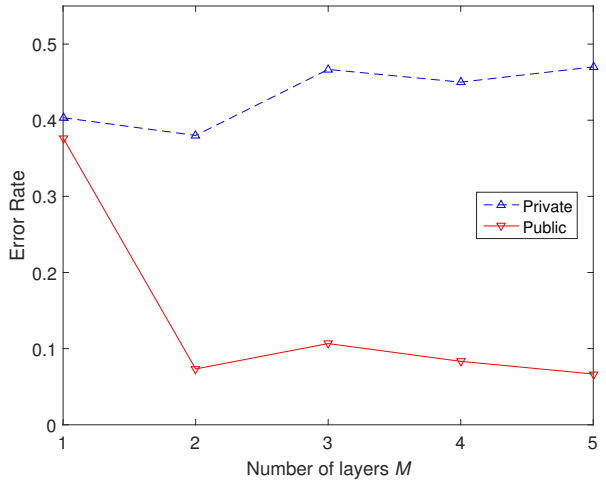


(a) The impact of the number of layers $M$ on public and private hypothesis error rates.

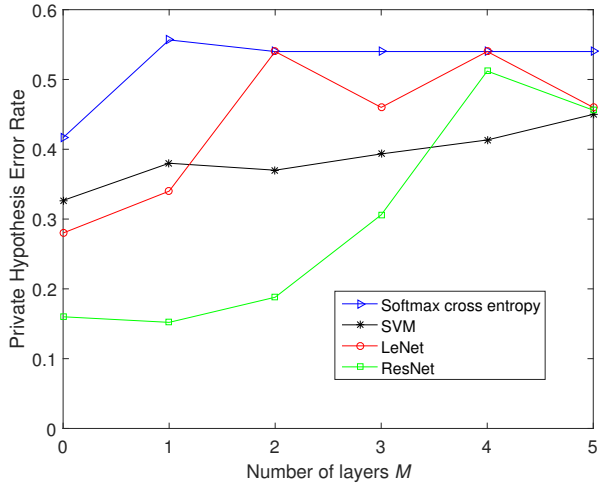


(b) The private hypothesis error rate under different learning techniques. Zero layer indicates that the learning is applied on the raw sensor observations.

Fig. 12. MNPT for images with three types of gun and cash.

empirical risk minimization problem, and provided empirical experiments that verify the performance of our approach.

## Appendix A
## Proof of Theorem 1

The proof proceeds similarly as that for Theorem 1 and 2 in [34], and we present only an outline of the essential adaptations here. Let

$$\ell(\mathbf{z}) = \frac{\mathsf{p}_{\mathbf{Z}|q}(\mathbf{z} \mid 1)}{\mathsf{p}_{\mathbf{Z}|q}(\mathbf{z} \mid -1)} \tag{39}$$

be the likelihood ratio function. We first show the following lemma.

**Lemma A.1.** *Suppose that* $\gamma(\mathbf{Z}) = 1$ *if* $\ell(\mathbf{Z}) \geq 1$ *and* $\gamma(\mathbf{Z}) = -1$ *otherwise. If* $R(\gamma) = \frac{1}{2}\left(\mathbb{P}\left(\gamma(\mathbf{Z}) = -1 \mid q = 1\right) + \mathbb{P}\left(\gamma(\mathbf{Z}) = 1 \mid q = -1\right)\right) \geq \theta \in [0, 1/2]$, *then for any* $\delta > 0$, *there exists* $\xi > 0$ *such that* $q$ *given* $\mathbf{Z}$ *has* $(\epsilon, \delta)$*-information privacy with* $\epsilon = \log \frac{\xi}{(\xi + 2\theta - 1)_+}$.

*Proof:* If $-\infty < \ell(\mathbf{Z}) < \infty$ almost surely, then the result follows immediately from Theorem 1(ii) of [34]. On the other hand, suppose that $\ell(\mathbf{Z})$ is unbounded. Then, there exist $-\infty < \ell_* < 1 < \ell^* < \infty$ such that $\mathbb{P}\left(\ell_* < \ell(\mathbf{Z}) < \ell^*\right) \geq 1 - \delta$ and a positive $\xi = \min\{\mathbb{P}\left(\ell(\mathbf{Z}) \leq \ell_* \mid q = -1\right), \mathbb{P}\left(\ell(\mathbf{Z}) \geq \ell^* \mid q = 1\right)\} \leq \delta/2$. Proceeding in the same manner as the proof of Theorem 1(ii) in [34], we obtain the lemma. ∎

We now proceed with the proof of the theorem. We follow the same steps as in the proof of Theorem 2 in [34], except where the assumption that $\mathbf{Z}$ takes values from a finite alphabet is used. Specifically let $\tilde{q}$ be a binary hypothesis with uniform prior, and satisfies $\mathsf{p}_{\mathbf{Z}|\tilde{q}}(\mathbf{Z}|q') = \mathsf{p}_{\mathbf{Z}|q}(\mathbf{Z}|q')$ for all $\mathbf{Z} \in \mathbb{U}$ and $q' \in \{-1, 1\}$. Let $\gamma^*(\mathbf{Z}) = \arg\inf_{\iota \in \mathbb{R}} \left(\mathsf{p}_{\tilde{q}|\mathbf{Z}}(1 \mid \mathbf{Z})\phi(\iota) + \mathsf{p}_{\tilde{q}|\mathbf{Z}}(-1 \mid \mathbf{Z})\phi(-\iota)\right)$. We claim that there exists a $\gamma(\mathbf{Z}) \in \mathcal{H}$ such that $\gamma(\mathbf{Z}) = \gamma^*(\mathbf{Z})$ for all $\mathbf{Z} \in \mathbb{U}$, i.e., for some $\alpha_k \in \mathbb{R}$ and $\mathbf{Z}_k \in \mathbb{R}^{dkC}$, $k \geq 1$,

$$\sum_{k \geq 1} \alpha_k v(\mathbf{Z}) u(\mathbf{Z}_k^T \mathbf{Z} + b_k) = \gamma^*(\mathbf{Z}), \text{ or}$$

$$\sum_{k \geq 1} \alpha_k u(\mathbf{Z}_k^T \mathbf{Z} + b_k) = \frac{\gamma^*(\mathbf{Z})}{v(\mathbf{Z})}.$$

Since the set of functions $\{\sum_{k=1}^K \alpha_k u(\mathbf{r}_k^T \mathbf{Z} + b_k) : \alpha_k \in \mathbb{R}, \mathbf{r}_k \in \mathbb{R}^{dkC}, b_k \in \mathbb{R}, K \geq 1\}$ is dense in the space of continuous functions on $\mathbb{U}$ [44], our claim follows. The rest of the proof now follows the same argument as that for Theorem 2 in [34] with $\delta'$ in place of $\delta$ and Lemma A.1 in place of Theorem 1(ii).

## Appendix B
## Proof of Lower Bound (21)

From the Cauchy-Schwarz inequality, for any $\mathbf{G}$ and $\mathbf{G}'$ we have

$$\begin{aligned}
&\langle \nabla J_q(\mathbf{G}) - \nabla J_q(\mathbf{G}'), \mathbf{G} - \mathbf{G}' \rangle \\
&\geq -\|\nabla J_q(\mathbf{G}) - \nabla J_q(\mathbf{G}')\|_F \cdot \|\mathbf{G} - \mathbf{G}'\|_F \\
&\geq -L\|\mathbf{G} - \mathbf{G}'\|_F^2,
\end{aligned} \tag{40}$$

where the last inequality follows from Assumption 3. Let

$$g(\mathbf{G}) = \frac{L}{2}\|\mathbf{G}\|_F^2 + J_q(\mathbf{G}),$$

then its gradient is $\nabla g(\mathbf{G}) = L\mathbf{G} + \nabla J_q(\mathbf{G})$. From (40), we obtain

$$\begin{aligned}
&\langle \nabla g(\mathbf{G}) - \nabla g(\mathbf{G}'), \mathbf{G} - \mathbf{G}' \rangle = \\
&\langle \nabla J_q(\mathbf{G}) - \nabla J_q(\mathbf{G}'), \mathbf{G} - \mathbf{G}' \rangle + L\|\mathbf{G} - \mathbf{G}'\|_F^2 \geq 0.
\end{aligned}$$

Therefore, $g(\mathbf{G})$ is a convex function. The lower bound (21) then follows from and the first order condition $g(\mathbf{G}) \geq g(\mathbf{G}[n]) + \langle \nabla g(\mathbf{G}[n]), \mathbf{G} - \mathbf{G}[n] \rangle$, and the proof is complete.

## REFERENCES


[1] I. Butun, S. D. Morgera, and R. Sankar, "A survey of intrusion detection systems in wireless sensor networks," *IEEE Commun. Surveys & Tutorials*, vol. 16, no. 1, pp. 266–282, 2014.

[2] J. Chen, K. Kwong, D. Chang, J. Luk, and R. Bajcsy, "Wearable sensors for reliable fall detection," in *Proc. Annual Int. Conf. of the IEEE Engineering in Medicine and Biology Society*, 2006, pp. 3551–3554.

[3] W. P. Tay, J. N. Tsitsiklis, and M. Z. Win, "On the impact of node failures and unreliable communications in dense sensor networks," *IEEE Trans. Signal Process.*, vol. 56, no. 6, pp. 2535 – 2546, Jun. 2008.

[4] H. Alemdar and C. Ersoy, "Wireless sensor networks for healthcare: A survey," *Computer Networks*, vol. 54, no. 15, pp. 2688–2710, 2010.

[5] W. P. Tay, J. N. Tsitsiklis, and M. Z. Win, "Data fusion trees for detection: Does architecture matter?" *IEEE Trans. Inf. Theory*, vol. 54, no. 9, pp. 4155 – 4168, Sep. 2008.

[6] H. Chen, B. Chen, and P. Varshney, "A new framework for distributed detection with conditionally dependent observations," *IEEE Trans. Signal Process.*, vol. 60, no. 3, pp. 1409 –1419, Mar. 2012.

[7] W. P. Tay, "Whose opinion to follow in multihypothesis social learning? A large deviations perspective," *IEEE J. Sel. Topics Signal Process.*, vol. 9, no. 2, pp. 344 – 359, Mar. 2015.

[8] J. Ho, W. P. Tay, T. Q. S. Quek, and E. K. P. Chong, "Robust decentralized detection and social learning in tandem networks," *IEEE Trans. Signal Process.*, vol. 63, no. 19, pp. 5019 – 5032, Oct. 2015.

[9] J. Evans, "What apple users need to know about differential privacy," www.computerworld.com, Jun. 2016.

[10] D. Boneh, E.-J. Goh, and K. Nissim, "Evaluating 2-DNF formulas on ciphertexts," in *Proc. Int. Conf. on Theory of Cryptography*, Cambridge, MA, 2005, pp. 325–341.

[11] Y. Ishai and A. Paskin, "Evaluating branching programs on encrypted data," in *Proc. Int. Conf. on Theory of Cryptography*, Berlin, Heidelberg, 2007, pp. 575–594.

[12] C. Gentry, "Fully homomorphic encryption using ideal lattices," in *Proc. Annual ACM Symp. on Theory of Computing*. New York, NY, USA: ACM, 2009, pp. 169–178.

[13] C. Dwork, "Differential privacy: A survey of results," in *Proc. Int. Conf. Theory and Applications of Models of Computation*, Xi'an, 2008, pp. 1–19.

[14] A. Friedman and A. Schuster, "Data mining with differential privacy," Washington, DC, 2010, pp. 493–502.

[15] M. E. Andrés, N. E. Bordenabe, K. Chatzikokolakis, and C. Palamidessi, "Geo-indistinguishability: Differential privacy for location-based systems," in *Proc. ACM SIGSAC Conf. on Computer & Commun. Security*, Berlin, 2013, pp. 901–914.

[16] R. Chen, B. C. Fung, S. Y. Philip, and B. C. Desai, "Correlated network data publication via differential privacy," *Int. J. on Very Large Data Bases*, vol. 23, no. 4, pp. 653–676, Nov. 2014.

[17] J. C. Duchi, M. I. Jordan, and M. J. Wainwright, "Local privacy and statistical minimax rates," in *Proc. IEEE Symp. on Foundations of Computer Science*, Berkeley, 2013, pp. 429–438.

[18] L. Wassermana and S. Zhou, "A statistical framework for differential privacy," *Journal of the American Statistical Association*, vol. 105, no. 489, pp. 375–389, 2010.

[19] Y. Ishai and A. Paskin, "Evaluating branching programs on encrypted data," in *Theory of Cryptography Conference*, 2007.

[20] J. Yu, B. Zhang, Z. Kuang, D. Lin, and J. Fan, "iprivacy: Image privacy protection by identifying sensitive objects via deep multi-task learning," *IEEE Trans. Information Forensics and Security*, vol. 12, no. 5, pp. 1005–1016, 2017.

[21] F. Calmon and N. Fawaz, "Privacy against statistical inference," in *Proc. Allerton Conf. Commun., Control, Comput.*, 2012.

[22] J. Hamm, "Preserving privacy of continuous high-dimensional data with minimax filters," in *Int. Conf. Artificial Intelligence and Statistics*, 2015.

[23] ——, "Enhancing utility and privacy with noisy minimax filters," in *Proc. IEEE Int. Conf. Acoustics, Speech, and Signal Processing*, 2017.

[24] K. Diamantaras and S.-Y. Kung, "Data privacy protection by kernel subspace projection and generalized eigenvalue decomposition," in *IEEE Int. Workshop Machine Learning for Signal Processing*, Salerno, 2016, pp. 1–6.

[25] M. Al, S. Wan, and S.-Y. Kung, "Ratio utility and cost analysis for privacy preserving subspace projection," *arXiv preprint arXiv:1702.07976*, 2017.

[26] M. Sun and W. P. Tay, "Privacy-preserving nonparametric decentralized detection," in *Proc. IEEE Int. Conf. Acoustics, Speech, and Signal Processing*, Shanghai, China, Mar. 2016.

[27] X. He, W. P. Tay, and M. Sun, "Privacy-aware decentralized detection using linear precoding," in *Proc. IEEE Sensor Array and Multichannel Signal Processing Workshop*, July 2016.

[28] Y. Bengio, *Learning Deep Architectures for AI*. Hanover, MA, USA: Now Publishers Inc., Jan. 2009, vol. 2, no. 1.

[29] G. Hinton, L. Deng, D. Yu, G. E. Dahl, A. r. Mohamed, N. Jaitly, A. Senior, V. Vanhoucke, P. Nguyen, T. N. Sainath, and B. Kingsbury, "Deep neural networks for acoustic modeling in speech recognition: The shared views of four research groups," *IEEE Signal Processing Magazine*, vol. 29, no. 6, pp. 82–97, 2012.

[30] X. He and W. P. Tay, "Multilayer sensor network for information privacy," in *Proc. IEEE Int. Conf. Acoustics, Speech, and Signal Processing*, Mar. 2017.

[31] V. Vapnik, *The Nature of Statistical Learning Theory*. Springer-Verlag New York, 2000.

[32] T. Zhang, "Statistical behavior and consistency of classification methods based on convex risk minimization," *Annals of Statistics*, pp. 56–85, 2004.

[33] X. Nguyen, M. J. Wainwright, and M. I. Jordan, "Nonparametric decentralized detection using kernel methods," *IEEE Trans. Signal Process.*, vol. 53, no. 11, pp. 4053–4066, Nov 2005.

[34] M. Sun, W. P. Tay, and X. He, "Towards information privacy for the Internet of Things," *submitted to IEEE Trans. Signal Process.*, 2016. [Online]. Available: https://arxiv.org/abs/1611.04254

[35] A. Beck and M. Teboulle, "Mirror descent and nonlinear projected subgradient methods for convex optimization," *Oper. Res. Lett.*, vol. 31, no. 3, pp. 167–175, May 2003.

[36] L. Vandenberghe, "Gradient method," 2016. [Online]. Available: http://www.seas.ucla.edu/~vandenbe/236C/lectures/gradient.pdf

[37] R. Chavarriaga, H. Sagha, A. Calatroni, S. Digumarti, G. Tröster, J. Millán, and D. Roggen, "The opportunity challenge: A benchmark database for on-body sensor-based activity recognition," *Pattern Recognition Letters*, 2013.

[38] C. Chen, R. Jafari, and N. Kehtarnavaz, "Utd-mhad: A multimodal dataset for human action recognition utilizing a depth camera and a wearable inertial sensor," in *Proc. of IEEE Int. Conf. on Image Processing*, 2015.

[39] X. He, W. P. Tay, and M. Sun, "Gun and cash images," 2017. [Online]. Available: http://dx.doi.org/10.21979/N9/OTHTTC

[40] Y. Lecun, L. Bottou, Y. Bengio, and P. Haffner, "Gradient-based learning applied to document recognition," *Proc. of the IEEE*, vol. 86, no. 11, pp. 2278–2324, Nov 1998.

[41] L. Deng, *Connecting Deep Learning Features to Log-Linear Models*. MIT Press, August 2015. [Online]. Available: https://www.microsoft.com/en-us/research/publication/connecting-deep-learning-features-to-log-linear-models/

[42] K. He, X. Zhang, S. Ren, and J. Sun, "Deep residual learning for image recognition," in *IEEE Conf. on Computer Vision and Pattern Recognition*, 2016.

[43] X. Glorot, A. Bordes, and Y. Bengio, "Deep sparse rectifier neural networks," in *Proc. Int. Conf. on Artificial Intelligence and Statistics*, Florida, USA, 2011, pp. 315–323.

[44] M. Leshno, Y. V. Lin, A. Pinkus, and S. Schocken, "Multilayer feedforward networks with a non-polynomial activation function can approximate any function," *Neural Networks*, vol. 6, pp. 861–867, 1993.